Journal of
Applied Physics

ARTICLE

pubs.aip.org/aip/jap

Oxygenates production in a microfluidic dielectric barrier discharge device sustained in $Ar/CH_4/O_2$

Cite as: J. Appl. Phys. **137**, 013301 (2025); doi: 10.1063/5.0239464
Submitted: 19 September 2024 · Accepted: 16 December 2024 ·
Published Online: 3 January 2025

View Online

Export Citation

CrossMark

Mackenzie Meyer,[1,a),b)] Ryan Hartman,[2,c)] and Mark J. Kushner[1,d)]

AFFILIATIONS

[1]Electrical Engineering and Computer Science Department, University of Michigan, 1301 Beal Ave., Ann Arbor, Michigan 48109-2122, USA
[2]Department of Chemical and Biomolecular Engineering, New York University, New York, New York 11201, USA

[a)]**Present address:** NRC Postdoctoral Research Associate, Plasma Physics Division, US Naval Research Laboratory, 4555 Overlook Ave. SW, Washington, DC 20375, USA
[b)]maemeyer@umich.edu
[c)]ryan.hartman@nyu.edu
[d)]**Author to whom correspondence should be addressed:** mjkush@umich.edu

03 January 2025 12:38:27

ABSTRACT

Reforming of methane (CH_4) is a process to produce syngas (CO/H_2) and other value-added chemicals including oxygenates such as methanol (CH_3OH). Atmospheric pressure plasmas have the potential to be more energy efficient than traditional reforming methods as value-added chemicals can be synthesized directly in the plasma without requiring an additional step. In this paper, we discuss the results from a computational investigation of the formation of oxygenates by CH_4 oxidation in the presence of Ar, including CH_3OH and CH_2O, in a nanosecond pulsed dielectric barrier discharge. The plasma is formed in a microfluidic channel whose small dimensions are ideal for plasma formation at atmospheric pressure. The production and consumption mechanisms of dominant radicals and long-lived species are discussed in detail for the base case conditions of $Ar/CH_4/O_2 = 50/25/25$. CH_3OH is produced primarily by CH_3O reacting with CH_3O and CH_3O_2 reacting with OH, while CH_2O formation relies on reactions involving CH_3O and CH_3. The most abundant oxygenate formed is CO (produced by H abstraction from CHO). However, the greenhouse gas CO_2 is also formed as a by-product. The effects of gas mixture are examined to maximize the CH_3OH and CH_2O densities while decreasing the CO_2 density. Increasing the Ar percentage from 0% to 95% decreased the CH_3OH and CH_2O densities. At low Ar percentages, this is due to an increase in consumption of CH_3OH and CH_2O, while at high Ar percentages (>40% Ar), the production of CH_3OH and CH_2O is decreased. However, both CO and CO_2 reached peak densities at 70%–90% Ar. Changing the CH_4/O_2 ratio while keeping 50% Ar in the discharge led to increased CH_3OH and CH_2O production, reaching peak densities at 35%–40% CH_4. The CO and CO_2 densities decreased beyond 20% CH_4, indicating that a CH_4 rich discharge is ideal for forming the desired oxygenates.

© 2025 Author(s). All article content, except where otherwise noted, is licensed under a Creative Commons Attribution-NonCommercial 4.0 International (CC BY-NC) license (https://creativecommons.org/licenses/by-nc/4.0/). https://doi.org/10.1063/5.0239464

I. INTRODUCTION

Reforming of methane (CH_4) is a chemical process used widely to produce syngas, a mixture of carbon monoxide (CO) and hydrogen (H_2). CH_4 reforming can be performed through two processes—steam reforming in the presence of H_2O and dry reforming in the presence of CO_2.[1] While steam reforming of CH_4 is commonly used in industrial processes, it is an endothermic process requiring elevated pressures and temperatures.[1] The syngas produced in steam reforming of CH_4 is often further converted to other value-added compounds. One of the most common value-added compounds produced is methanol (CH_3OH).[2] From CH_3OH, formaldehyde (CH_2O) is produced by oxidation.

Atmospheric pressure plasmas, when sustained in CH_4, convert CH_4 to other compounds.[3–7] Previous research has examined dry reforming of CH_4 in plasmas, where CH_4 and CO_2 are

converted to syngas and other compounds.[8–15] Plasmas have the potential to be more energy efficient than other CH_4 reforming processes as plasmas can be sustained near ambient temperature and at atmospheric pressure. Hot (several eV) electrons dissociate and ionize the neutral feedstock gases, leading to complex plasma chemistry while retaining low gas temperatures. CH_4 conversion proceeds through direct electron-impact dissociation of CH_4 or reactions of other plasma-produced radicals and excited states with CH_4, while the low gas temperature enables selectivity.

Conversion of CH_4 in the presence of a noble gas has been previously investigated.[16–19] Janeco *et al.* examined electron kinetics in $He/CH_4/CO_2$ mixtures and showed that addition of He shifted the electron energy distribution to higher energies.[20] The higher energy electrons led to increased conversion of CH_4 and CO_2. Rahmani and Nikravech showed that addition of Ar increased the electron density and electron temperature in CH_4/CO_2 mixtures.[21] Jo *et al.* showed that the identity of the noble gas (He, Ne, Ar, Kr, or Xe) affected the electron temperature and density.[22] Ozkan *et al.* examined the difference in CH_4 and CO_2 conversion in the presence of either Ar or He.[12] They showed that the conversion of CH_4 was higher for He than for Ar, while the conversion of CO_2 was higher for Ar than He.

Studies have also focused on the production of oxygenates, including CH_3OH and CH_2O.[23] De Bie *et al.* modeled the production of oxygenates in CH_4/O_2 mixtures and CH_4/CO_2 mixtures in a nanosecond pulsed dielectric barrier discharge (DBD).[24] They predicted the formation of many oxygenated species, including CH_3OH, CH_3OOH, CH_2O, C_2H_5OOH, C_2H_5OH, and CH_3CHO. Biswas *et al.* examined the production of oxygenates from CO_2 and C_2H_6.[25] The dominant product was CO, and other hydrocarbons and oxygenated species were also formed. Kolb *et al.* investigated the production of oxygenates in a DBD with 97% He.[26] The addition of O_2 to $He/CH_4/CO_2$ was shown to increase CH_3OH and CH_2O yields. Li *et al.* examined oxygenate production from $CH_4/CO_2/O_2$ discharges.[27] The increased amounts of O, OH, and HO_2 were responsible for enhancing the oxygenate production with O_2 addition. Oxygenate production in plasma-catalytic systems has also been studied.[28–30]

As we advance our knowledge of oxygenate production from CH_4 plasmas, the manner of implementing those processes also becomes important. That implementation should consider the method of excitation (e.g., DBD, microwave, glow, pulsing) and throughput. For example, pulsed ns DBDs have some advantages over microwave excitation when maintaining low gas temperatures, which is an important consideration in the conversion process. Micro-plasmas have the advantage of rapidly rising voltage pulses, well-controlled power deposition, and temperature control. DBD plasmas sustained in micro-channels (as found in microfluidic devices) enable such control as well as management of products through, for example, solvation into solution. Large throughput is achieved by parallel processing.

In this study, we used the 0-dimensional (0D) model *GlobalKin* to assess the production of CH_3OH and CH_2O in a pulsed nanosecond DBD sustained in $Ar/CH_4/O_2$ flowing through a microfluidic channel, ideal for producing uniform flows with high power deposition at atmospheric pressure. The goal is to examine mechanisms for CH_3OH and CH_2O production while minimizing the production of the greenhouse gas CO_2. The dominant production and consumption mechanisms of the plasma-produced radicals and long-lived species are identified. Common oxygenates formed include CH_3OH, CH_2O, and CO. The plasma-produced species that do not contain oxygen include H_2, C_2H_4, and C_2H_6. After examining the base case, the consequences of the gas mixture are examined. When increasing the Ar content while keeping $CH_4/O_2 = 1/1$, CH_3OH and CH_2O densities decrease while the density of CO_2 increases to 90% Ar. A mixture of 50% Ar and 35%–40% CH_4 (10%–15% O_2) maximizes CH_3OH and CH_2O production while also minimizing the amount of CO_2 formed.

The model is described in Sec. II. The results of the base case are discussed in Sec. III, including delineation of the production and consumption mechanisms of abundant radicals and long-lived species. Consequences of the gas mixture are discussed in Sec. IV, and conversion and energy expenditures are discussed in Sec. V. Concluding remarks are presented in Sec. VI.

II. DESCRIPTION OF MODEL

GlobalKin is a 0D plasma chemistry model that integrates continuity equations for neutral and charged species.[31] Sources and losses for these species include chemical reactions, flow, and diffusion to bounding surfaces of the plasma. Electron temperature T_e and gas temperature T_{gas} are calculated using their respective energy equations. A stationary solution of Boltzmann's equation produced using a two-term spherical harmonic expansion is used to compute the electron energy distribution at different values of E/N (electric field/gas number density). The resulting values of electron temperature T_e are then the basis of creating a look-up table of electron-impact rate coefficients and transport coefficients as a function of T_e. The look-up table is updated at the beginning of each discharge pulse by recomputing the electron energy distributions to reflect the changes in the gas mole fractions.

The gas mixture examined is $Ar/CH_4/O_2$, and the base case conditions are $Ar/CH_4/O_2 = 50/25/25$. The reaction mechanism includes 122 species, listed in Table I, and 3265 reactions between those species. The $Ar/O_2/H_2O$ mechanism is based on Van Gaens and Bogaerts,[32] and the $Ar/CH_4/H_2O$ mechanism is based on our previous work.[33] Additional reactions between hydrocarbon species and oxygen species were added to the mechanism and are listed in the supplementary material. Important reactions in the production and consumption of radicals and long-lived species are listed in Tables II and III, respectively. These reactions will be discussed in the following section.

The geometry in this work replicates that of our previous study of methyl radical production in a microfluidic channel.[33] The microfluidic channel serves as a dielectric barrier discharge (DBD). The channel dimensions are $500 \times 500\,\mu m^2$. The power is pulsed on ns timescales, ramping up over 15 ns, staying constant for 30–45 ns, and decreasing to 0 W at 60 ns. The peak power deposition is $228\,kW\,cm^{-3}$, and the energy deposited into the plasma is $10\,mJ\,cm^{-3}$ per pulse. The pulse repetition rate is 10 kHz (0.1 ms period), and the evolution over 20 pulses (2 ms) was tracked. The flow rate is 0.1 SCCM to approximate plug flow, and the outflow was adjusted to maintain 1 atm at a timescale of 0.1 ms.

Since *GlobalKin* is a 0D model, it does not account for spatial dynamics such as ionization waves in the bulk plasmas or along

03 January 2025 12:38:27

© Author(s) 2025

TABLE I. Species included in the reaction mechanism.

e, Ar, Ar($1s_1$), Ar($1s_2$), Ar($1s_3$), Ar($1s_4$), Ar(4P), Ar(4D), Ar^+, Ar_2*, Ar_2^+, ArH^+
H, H*, H^+, H^-, H_2, H_2(r), H_2(v), H_2*, H_2^+, H_3^+
H_2O, H_2O(v), H_2O^+, H_3O^+, OH, OH*, OH^+, OH^-, HO_2, H_2O_2, $H_2O^+(H_2O)$, $O_2^+(H_2O)$, $H_3O^+(H_2O)$, $O_2^-(H_2O)$, $O_2^-(H_2O)_2$, $O^-(H_2O)$, $OH^-(H_2O)$, $OH^-(H_2O)_2$
O_2, O_2(v), O_2(r), $O_2(^1\Delta)$, $O_2(^1\Sigma)$, O_2^+, O_2^-, O_4^+, O, $O(^1D)$, O^+, O^-, O_3, O_3*, O_3^-
CH_4, CH_4(v), CH_4^+, CH_5^+, CH_3, CH_3(v), CH_3^+, CH_2, CH_2(v), CH_2^+, CH_2^-, CH, CH^+, C, C^+
C_2H_6, C_2H_6(v), $C_2H_6^+$, C_2H_5, $C_2H_5^+$, C_2H_4, $C_2H_4^+$, C_2H_3, $C_2H_3^+$, C_2H_2, $C_2H_2^+$, $C_2H_2^-$, C_2H, C_2H^+, C_2, C_2^+
C_3H_8, C_3H_7N (*n*-propyl radical), C_3H_7I (iso-propyl radical), C_3H_6, C_3H_5, C_3H_4, C_3H_3, C_3H_2
CHO, CHO^+, CH_2O, CH_2O^+, CH_3O, CH_3O^+, CH_2OH, CH_2OH^+, CH_3OH, CH_3OH^+, $CH_3OH_2^+$ CH_3OOH, CH_3O_2
CO, CO(v), CO^+, CO_2, CO_2(v), CO_2^+
C_2H_5OH, C_2H_5O, C_2H_5OOH, $C_2H_5O_2$, CH_3CO, CH_2CO, CH_3CHO, CH_2CHO, C_2HO

surfaces. The computational expediency of global models is that they enable detailed analysis of the plasma chemistry and can be used to compute plasma chemical dynamics over multiple pulses and long time scales. We acknowledge that chemical conversion processes that depend on the specifics of these spatial dynamics will not be captured in a global model. However, we expect that the trends predicted by global models will hold for higher dimensional models and experiments.

III. OXYGENATED SPECIES PRODUCTION

In this section, the radical and long-lived species production and consumption for the base case of $Ar/CH_4/O_2 = 50/25/25$ are discussed. The plasma properties are discussed in Sec. III A. The production and consumption mechanisms of radicals and long-lived species are discussed in Secs. III B and III C, respectively.

A. Plasma properties

The plasma properties are shown in Fig. 1 over the last of 20 pulses. The electrons are initially seeded with a density of $10^9\,cm^{-3}$ at the beginning of each discharge pulse. As power is applied with this initially small electron density, T_e increases to 4.9 eV, above the quasi-steady-state value, to sustain an electron avalanche. With the increase in electron density, T_e decreases. During the constant power portion of the pulse, the electron density and T_e reach their quasi-steady state values of $1.8\times10^{13}\,cm^{-3}$ and 3.1 eV. As the power decreases at the end of the pulse, T_e rapidly decreases to lower the power dissipation per electron. Electrons rapidly recombine with positive ions, dominantly dissociative recombination, or attach to form negative ions including OH^-, O_2^-, and O^-. The gas temperature increases from its initial value of 300 K up to 403 K at 2 ms.

B. Radical production and consumption

The dominant radicals formed in the $Ar/CH_4/O_2$ system are shown in Fig. 2, and the production and consumption reactions of each radical are detailed in Table II for those processes that contribute more than 5% of the total production or consumption of the radical. The most important reactions will be discussed in this section.

The reactive oxygen species (ROS) radicals are shown in Fig. 2(a). Since there is a large fraction of O_2 in the gas, O is the most abundant ROS radical formed. O is formed through electron-impact of O_2 (61% of O production over the 20 pulses) as well as through

$$HO_2 + O_2^* \rightarrow OH + O_2 + O, \tag{1}$$

thereby producing 25% of the O produced over the 20 pulses. O is consumed through three-body formation of O_3 (40%) and formation of O_2 with other radicals including CH_3O_2, HO_2, OH, and CH_3O. H is also produced, primarily from the electron-impact of CH_4 (34%) and

$$OH + O \rightarrow H + O_2, \tag{2}$$

thereby contributing 28% of H production over 20 pulses. H is consumed by three-body recombination with O_2 forming HO_2 (67%). While O and H are formed from direct electron-impact reactions with the feedstock gases O_2 and CH_4, HO_2, and OH rely on those radicals to be generated first. As a result, HO_2 and OH reach their maximum densities after the discharge pulse, while the densities of O and H peak as the pulse ends. HO_2 is dominantly produced by three-body recombination of H and O_2 (42%), though 30% of HO_2 is produced by

$$CHO + O_2 \rightarrow CO + HO_2. \tag{3}$$

HO_2 remains at an elevated density between the pulses, reaching $6.7\times10^{14}\,cm^{-3}$ before the final pulse. HO_2 is consumed in reactions with $O_2^{(1\Delta)}$ (56%) and O (32%). Both $O_2^{(1\Delta)}$ and O are produced during the pulse and consumed in the afterglow, decreasing the amount of HO_2 consumed in the afterglow. OH relies on HO_2 to be produced, both through reactions with $O_2^{(1\Delta)}$ (45%) and formation of O_2 from HO_2 (26%). OH is consumed in H abstraction from CH_4 (25%) and CH_2O (20%).

The dominant hydrocarbon radicals are shown in Fig. 2(b) over the last of 20 pulses. CH_3 is the most abundant hydrocarbon radical, produced by H abstraction from CH_4 by OH (39%), electron-impact dissociation of CH_4 (26%), and O reacting with CH_3O (18%). CH_3 is primarily consumed in association with O_2 to form CH_3O_2 (87%), operating in the high-pressure limit. The next most abundant hydrocarbon radical is CH_2, a lumped state of the triplet and singlet states. CH_2 is formed by the electron-impact dissociation of CH_4 (60%) as well as dissociative excitation transfer (DET) from the Ar(4s) multiplet (Ar($1s_1$), Ar($1s_2$), Ar($1s_3$), Ar ($1s_4$)) to CH_4 (26%). Higher energy Ar states including Ar(4P) and Ar(4D) directly ionize CH_4 instead of dissociating CH_4. DET also contributes to CH_3 production. The integrated rate of DET to form CH_2 is double that of CH_3, but the contribution of DET to CH_3 formation is low (1%) as there are other pathways to form CH_3.

03 January 2025 12:38:27

© Author(s) 2025

TABLE II. Dominant production and consumption mechanisms of radicals produced in $Ar/CH_4/O_2$ = 50/25/25. Production and consumption reactions are listed if they contribute more than 5% of the total production and consumption over 20 pulses.

Production reactions	Integrated contribution to production over 20 pulses (cm^{-3})	Consumption reactions	Integrated contribution to consumption over 20 pulses (cm^{-3})
O			
$e + O_2 \rightarrow O + O + e$	1.8×10^{17} (61%)	$O + O_2 + M \rightarrow O_3/O_3^* + M$, $M = CH_4$, Ar, O_2, O_3, H_2O	1.2×10^{17} (40%)
$HO_2 + O_2^{(1\Delta)} \rightarrow OH + O_2 + O$	7.2×10^{16} (25%)	$CH_3O_2 + O \rightarrow CH_3O + O_2$	5.5×10^{16} (19%)
		$HO_2 + O \rightarrow OH + O_2$	4.1×10^{16} (14%)
		$OH + O \rightarrow H + O_2$	2.2×10^{16} (7.5%)
		$CH_3O + O \rightarrow CH_3 + O_2$	1.9×10^{16} (6.5%)
H			
$e + CH_4 \rightarrow CH_3 + H + e$	2.7×10^{16} (34%)	$H + O_2 + M \rightarrow HO_2 + M$, $M = CH_4$, Ar, O_2, O_3, H_2O	5.4×10^{16} (67%)
$OH + O \rightarrow H + O_2$	2.2×10^{16} (28%)	$H + O_3 \rightarrow OH + O_2$	1.8×10^{16} (22%)
$CH_3 + O \rightarrow CH_2O + H$	6.4×10^{15} (8.0%)		
$CH_3OH + OH \rightarrow CH_2O + H_2O + H$	4.7×10^{15} (5.8%)		
HO_2			
$H + O_2 + M \rightarrow HO_2 + M$, $M = CH_4$, Ar, O_2, O_3, H_2O	5.4×10^{16} (42%)	$HO_2 + O_2^{(1\Delta)} \rightarrow OH + O_2 + O$	7.2×10^{16} (56%)
$CHO + O_2 \rightarrow CO + HO_2$	3.9×10^{16} (30%)	$HO_2 + O \rightarrow OH + O_2$	4.2×10^{16} (32%)
$CH_3O_2 + OH \rightarrow CH_3O + HO_2$	1.5×10^{16} (12%)		
$CH_3O + O_2 \rightarrow CH_2O + HO_2$	8.6×10^{15} (6.6%)		
OH			
$HO_2 + O_2^{(1\Delta)} \rightarrow OH + O_2 + O$	7.2×10^{16} (45%)	$CH_4 + OH \rightarrow CH_3 + H_2O$	4.0×10^{16} (25%)
$HO_2 + O \rightarrow OH + O_2$	4.1×10^{16} (26%)	$CH_2O + OH \rightarrow CHO + H_2O$	3.2×10^{16} (20%)
$H + O_3 \rightarrow OH + O_2$	1.8×10^{16} (11%)	$OH + O \rightarrow H + O_2$	2.2×10^{16} (14%)
		$CH_3O_2 + OH \rightarrow CH_3O + HO_2$	1.5×10^{16} (9.5%)
		$CH_3O_2 + OH \rightarrow CH_3OH + O_2$	1.5×10^{16} (9.5%)
CH_3			
$CH_4 + OH \rightarrow CH_3 + H_2O$	4.0×10^{16} (39%)	$CH_3 + O_2 \rightarrow CH_3O_2$	9.1×10^{16} (87%)
$e + CH_4 \rightarrow CH_3 + H + e$	2.8×10^{16} (26%)	$CH_3 + O \rightarrow CH_2O + H$	6.4×10^{15} (6.2%)
$CH_3O + O \rightarrow CH_3 + O_2$	1.9×10^{16} (18%)		
$CH_2 + CH_4 \rightarrow CH_3 + CH_3$	7.0×10^{15} (6.7%)		
CH_2			
$e + CH_4 \rightarrow CH_2 + H_2 + e$	4.6×10^{15} (60%)	$CH_2 + CH_4 \rightarrow C_2H_5 + H$	3.5×10^{15} (46%)
$Ar^* + CH_4 \rightarrow CH_2 + H + H + Ar$, $Ar^* = Ar(1s_1)$, $Ar(1s_2)$, $Ar(1s_3)$, $Ar(1s_4)$	2.0×10^{15} (26%)	$CH_2 + CH_4 \rightarrow CH_3 + CH_3$	3.5×10^{15} (46%)
$CH + CH_4 \rightarrow CH_2 + CH_3$	7.8×10^{14} (10%)		
CH			
$e + CH_4 \rightarrow CH + H_2 + H + e$	2.3×10^{15} (99%)	$CH + CH_4 \rightarrow CH_3 + CH_2$	7.7×10^{14} (33%)
		$CH + CH_4 \rightarrow C_2H_4 + H$	7.7×10^{14} (33%)
		$CH + O_2 \rightarrow CO + O + H$	2.3×10^{14} (10%)
		$CH + O_2 \rightarrow CO_2 + H$	2.3×10^{14} (10%)
		$CH + O_2 \rightarrow CHO + O$	1.5×10^{14} (7%)
		$CH + O_2 \rightarrow CO + OH$	1.5×10^{14} (7%)
C_2H_5			
$CH_2 + CH_4 \rightarrow C_2H_5 + H$	3.5×10^{15} (98%)	$C_2H_5 + O_2 \rightarrow C_2H_5O_2$	3.4×10^{15} (95%)

03 January 2025 12:38:27

© Author(s) 2025

TABLE II. (*Continued.*)

Production reactions	Integrated contribution to production over 20 pulses (cm^{-3})	Consumption reactions	Integrated contribution to consumption over 20 pulses (cm^{-3})
CH_3O_2			
$CH_3 + O_2 \rightarrow CH_3O_2$	9.1×10^{16} (99%)	$CH_3O_2 + O \rightarrow CH_3O + O_2$	5.5×10^{16} (60%)
		$CH_3O_2 + OH \rightarrow CH_3O + HO_2$	1.5×10^{16} (17%)
		$CH_3O_2 + OH \rightarrow CH_3OH + O_2$	1.5×10^{16} (17%)
CH_3O			
$CH_3O_2 + O \rightarrow CH_3O + O_2$	5.5×10^{16} (72%)	$CH_3O + CH_3O \rightarrow CH_2O + CH_3OH$	3.6×10^{16} (47%)
$CH_3O_2 + OH \rightarrow CH_3O + HO_2$	1.5×10^{16} (20%)	$CH_3O + O \rightarrow CH_3 + O_2$	1.9×10^{16} (25%)
		$CH_3O + O_2 \rightarrow CH_2O + HO_2$	8.6×10^{15} (11%)
		$CH_3O + O \rightarrow CH_2O + OH$	7.6×10^{15} (9.9%)
		$CH_3O + OH \rightarrow CH_2O + H_2O$	4.2×10^{15} (5.5%)
CHO			
$CH_2O + OH \rightarrow CHO + H_2O$	3.2×10^{16} (80%)	$CHO + O_2 \rightarrow CO + HO_2$	3.9×10^{16} (98%)
$CH_2O + O \rightarrow CHO + OH$	7.4×10^{15} (19%)		
$C_2H_5O_2$			
$C_2H_5 + O_2 \rightarrow C_2H_5O_2$	3.4×10^{15} (97%)	$C_2H_5O_2 + OH \rightarrow C_2H_5O + HO_2$	2.3×10^{15} (67%)
		$C_2H_5O_2 + OH \rightarrow C_2H_5OH + O_2$	7.7×10^{14} (22%)
		$C_2H_5O_2 + HO_2 \rightarrow C_2H_5OOH + O_2$	3.5×10^{14} (10%)
C_2H_5O			
$C_2H_5O_2 + OH \rightarrow C_2H_5O + HO_2$	2.3×10^{15} (99%)	$C_2H_5O + O_2 \rightarrow CH_3CHO + HO_2$	2.2×10^{15} (95%)

CH_2 is consumed in reactions with CH_4, including

$$CH_2 + CH_4 \rightarrow CH_3 + CH_3, \tag{4}$$

$$CH_2 + CH_4 \rightarrow C_2H_5 + H. \tag{5}$$

Each of these reactions has a rate coefficient of $1.4 \times 10^{-11} \exp(-250\,K/T_{gas})\ cm^3/s$[34] and contributes 46% to CH_2 consumption. The final CH_x radical formed is CH, dominantly generated through the electron-impact dissociation of CH_4 (99%). CH is consumed in a wide variety of reactions, including those with CH_4 by

$$CH + CH_4 \rightarrow CH_3 + CH_2, \tag{6}$$

$$CH + CH_4 \rightarrow C_2H_4 + H. \tag{7}$$

Both of these reactions consume 33% of CH. The most abundant C_2H_x radical is C_2H_5, requiring other radicals to be formed before it can be produced. C_2H_5 is formed from CH_2 associating with CH_4 (reaction 5, 98%). C_2H_5 is primarily consumed in forming the oxygenated radical $C_2H_5O_2$ by association with O_2 (95%).

The oxygenated radicals are shown in Fig. 2(c). Contrary to the ROS and hydrocarbon radicals, all oxygenated radicals rely on other radicals for their formation. Therefore, their densities all reach their maxima after the discharge pulse, following the production of their precursors during the discharge pulse. The most abundant oxygenated radical is CH_3O_2, formed by the association of CH_3 and O_2 (99%). CH_3O_2 is primarily consumed in reactions with O (60%) and OH (34%), forming CH_3O and CH_3OH. Since CH_3O_2 is consumed in reactions with other radicals, CH_3O_2 persists between pulses with a density of $4.6 \times 10^{14}\ cm^{-3}$ at the end of 20 pulses.

To examine the products CH_3O_2 formation on longer timescales than the 0.1 ms between pulses, 0.3 s of afterglow following the 20th pulse was simulated. During that additional 0.3 s afterglow, CH_3O_2 reacts with itself in two processes, forming CH_3OH, CH_2O, CH_3O, and O_2. CH_3O_2 also reacts with HO_2, forming CH_3OOH and O_2. Reactions of CH_3O_2 with O and OH are reduced in importance as O and OH concentrations decrease substantially after the plasma pulses. CH_3O is the next most abundant oxygenated radical, formed through the same reactions that consume CH_3O_2. CH_3O is consumed by

$$CH_3O + CH_3O \rightarrow CH_2O + CH_3OH, \tag{8}$$

$$CH_3O + O \rightarrow CH_3 + O_2. \tag{9}$$

Reaction (8) consumes 47% of CH_3O, while reaction (9) consumes 25%. The final oxygenated radical with one C atom is CHO. CHO is formed by H abstraction from CH_2O by OH (80%) and O (19%). CHO is rapidly consumed in CO formation by H abstraction by O_2 (98%). Oxygenated radicals with two C atoms are also formed. Analogous to CH_3O_2, $C_2H_5O_2$ is formed through association reactions with C_2H_5 and O_2 (97%) and consumed in reactions

03 January 2025 12:38:27

© Author(s) 2025

TABLE III. Dominant production and consumption mechanisms of long-lived species produced in $Ar/CH_4/O_2$ = 50/25/25. Production reactions are listed if they contribute more than 5% of the total production over 20 pulses. Consumption mechanisms are only listed if their integrated rates are more than 5% of the integrated production rate of the species.

Production reactions	Integrated contribution to production over 20 pulses (cm^{-3})	Consumption reactions	Integrated contribution to consumption over 20 pulses (cm^{-3})
H_2O			
$CH_4 + OH \rightarrow CH_3 + H_2O$	4.0×10^{16} (40%)		
$CH_2O + OH \rightarrow CHO + H_2O$	3.2×10^{16} (31%)		
O_3			
$O + O_2 + M \rightarrow O_3 + M$, M = CH_4, Ar, O_2, O_3, H_2O	9.6×10^{16} (99.5%)	$H + O_3 \rightarrow OH + O_2$	1.8×10^{16} (38%)
		$O_2(^1\Sigma) + O_3 \rightarrow O_2 + O_2 + O$	1.3×10^{16} (28%)
H_2			
$e + CH_4 \rightarrow CH_2 + H_2 + e$	4.6×10^{15} (45%)		
$e + CH_4 \rightarrow CH + H_2 + H + e$	2.3×10^{15} (23%)		
$CH_3 + O \rightarrow CO + H_2 + H$	1.6×10^{15} (16%)		
$CH_3^+ + CH_4 \rightarrow C_2H_5^+ + H_2$	5.6×10^{14} (5.6%)		
H_2O_2			
$OH + OH + M \rightarrow H_2O_2 + M$, M = CH_4, Ar, O_2, H_2O, O_3	3.2×10^{15} (55%)	$OH + H_2O_2 \rightarrow H_2O + HO_2$	1.0×10^{15} (94%)
$HO_2 + HO_2 \rightarrow H_2O_2 + O_2$	2.5×10^{15} (41%)		
C_2H_4			
$CH + CH_4 \rightarrow C_2H_4 + H$	7.7×10^{14} (65%)		
$C_2H_5^+ + H_2O \rightarrow H_3O^+ + C_2H_4$	3.5×10^{14} (30%)		
C_2H_6			
$CH_3 + CH_3 \rightarrow C_2H_6$	2.2×10^{14} (98%)	$C_2H_6 + OH \rightarrow C_2H_5 + H_2O$	2.0×10^{13} (84%)
C_2H_2			
$e + C_2H_5^+ \rightarrow C_2H_2 + H_2 + H$	1.5×10^{13} (27%)	$C_2H_2 + O \rightarrow C_2HO + H$	1.3×10^{13} (70%)
$e + C_2H_5^+ \rightarrow C_2H_2 + H + H + H$	8.4×10^{12} (15%)	$C_2H_2 + O \rightarrow CO + CH_2$	3.1×10^{12} (18%)
$C_2H_4^+ + O_2^-(H_2O)_2 \rightarrow C_2H_2 + H + H + O_2 + H_2O + H_2O$	4.8×10^{12} (8.7%)		
$C_2H_4^+ + O_3^- \rightarrow C_2H_2 + H + H + O_3$	3.6×10^{12} (6.5%)		
$C_2H_3 + O_2 \rightarrow C_2H_2 + HO_2$	3.3×10^{12} (6.0%)		
C_3H_8			
$C_2H_5 + CH_3 \rightarrow C_3H_8$	6.3×10^{12} (99.3%)		
C_3H_6			
$C_2H_4 + CH_2 \rightarrow C_3H_6$	2.0×10^{12} (90%)	$C_3H_6 + O \rightarrow CHO + C_2H_5$	1.1×10^{12} (58%)
$C_2H_3 + CH_3 \rightarrow C_3H_6$	1.4×10^{11} (6.5%)	$C_3H_6 + O \rightarrow CH_2CO + CH_3 + H$	7.6×10^{11} (41%)
CO			
$CHO + O_2 \rightarrow CO + HO_2$	3.9×10^{16} (93%)		
CH_3OH			
$CH_3O + CH_3O \rightarrow CH_2O + CH_3OH$	1.8×10^{16} (53%)	$CH_3OH + OH \rightarrow CH_2O + H_2O + H$	4.7×10^{15} (45%)
$CH_3O_2 + OH \rightarrow CH_3OH + O_2$	1.5×10^{16} (45%)	$CH_3OH + OH \rightarrow CH_2OH + H_2O$	4.0×10^{15} (38%)
CH_2O			
$CH_3O + CH_3O \rightarrow CH_2O + CH_3OH$	1.8×10^{16} (32%)	$CH_2O + OH \rightarrow CHO + H_2O$	3.2×10^{16} (79%)
$CH_3O + O_2 \rightarrow CH_2O + HO_2$	8.6×10^{15} (15%)	$CH_2O + O \rightarrow CHO + OH$	7.4×10^{15} (18%)
$CH_3O + O \rightarrow CH_2O + OH$	7.8×10^{15} (13%)		
$CH_3 + O \rightarrow CH_2O + H$	6.4×10^{15} (11%)		

03 January 2025 12:38:27

© Author(s) 2025

TABLE III. (*Continued.*)

Production reactions	Integrated contribution to production over 20 pulses (cm^{-3})	Consumption reactions	Integrated contribution to consumption over 20 pulses (cm^{-3})
$CH_3OH + OH \rightarrow CH_2O + H_2O + H$	4.7×10^{15} (8.3%)		
$CH_2OH + O_2 \rightarrow CH_2O + HO_2$	4.7×10^{15} (8.3%)		
$CH_3O + OH \rightarrow CH_2O + H_2O$	4.2×10^{15} (7.5%)		
CO_2			
$CH_3CO + O \rightarrow CO_2 + CH_3$	9.4×10^{14} (33%)		
$OH + CO \rightarrow CO_2 + H$	6.8×10^{14} (24%)		
$CH + O_2 \rightarrow CO_2 + H$	2.3×10^{14} (8.1%)		
$CHO + O \rightarrow CO_2 + H$	2.1×10^{14} (7.4%)		
$CH_3CO + HO_2 \rightarrow CH_3 + CO_2 + OH$	2.0×10^{14} (7.1%)		
$CH_2 + O_2 \rightarrow CO_2 + H_2$	1.8×10^{14} (6.2%)		
CH_3OOH			
$CH_3O_2 + HO_2 \rightarrow CH_3OOH + O_2$	1.9×10^{15} (94%)	$CH_3OOH + OH \rightarrow CH_3O_2 + H_2O$	5.7×10^{14} (95%)
$CH_3O_2 + CH_3O \rightarrow CH_2O + CH_3OOH$	1.2×10^{14} (5.7%)		
C_2H_5OH			
$C_2H_5O_2 + OH \rightarrow C_2H_5OH + O_2$	7.7×10^{14} (96%)		
CH_3CHO			
$C_2H_5O + O_2 \rightarrow CH_3CHO + HO_2$	2.2×10^{15} (95%)	$CH_3CHO + OH \rightarrow CH_3CO + H_2O$	1.2×10^{15} (69%)
		$CH_3CHO + O \rightarrow OH + CH_3CO$	4.6×10^{14} (26%)
C_2H_5OOH			
$C_2H_5O_2 + HO_2 \rightarrow C_2H_5OOH + O_2$	3.5×10^{14} (91%)	$C_2H_5OOH + OH \rightarrow C_2H_5O_2 + H_2O$	6.8×10^{13} (58%)
$C_2H_5O_2 + C_2H_5O \rightarrow C_2H_5OOH + CH_3CHO$	3.3×10^{13} (8.6%)	$C_2H_5OOH + O \rightarrow C_2H_5O_2 + OH$	4.9×10^{13} (41%)

with OH

$$C_2H_5O_2 + OH \rightarrow C_2H_5O + HO_2, \quad (10)$$

$$C_2H_5O_2 + OH \rightarrow C_2H_5OH + O_2. \quad (11)$$

Reaction (10) contributes 69% to $C_2H_5O_2$ consumption and reaction (11) contributes 17%. C_2H_5O is formed by the reactions of $C_2H_5O_2$ and OH (99%), analogous to CH_3O. C_2H_5O is consumed by

$$C_2H_5O + O_2 \rightarrow CH_3CHO + HO_2, \quad (12)$$

contributing 95% of $C_2H_5O_2$ consumption.

C. Long-lived species

The long-lived species that are formed by repetitive pulsing are shown in Fig. 3, and the dominant production and consumption reactions of each long-lived species are listed in Table III. Consumption reactions appear in Table III if they represent more than 5% of the total integrated production rate of that long-lived species.

The long-lived species that do not contain carbon are shown in Fig. 3(a). The most abundant of these is H_2O, reaching $8.6 \times 10^{16}\,cm^{-3}$ (0.5% of the total density) at the end of 20 pulses. H_2O is formed by H abstraction by OH from CH_4 (40%) and CH_2O (31%). O_3 is also abundant in the discharge. O_3 is formed through three-body recombination of O and O_2 (99.5%). O_3 is consumed through

$$H + O_3 \rightarrow OH + O_2, \quad (13)$$

$$O_2(^1\Sigma) + O_3 \rightarrow O_2(^1\Delta) + O_2(^1\Delta) + O. \quad (14)$$

Reaction (13) contributes 38% to O_3 consumption, while reaction (14) contributes 28%. H_2 is formed through the electron-impact of CH_4 to form CH_2 (45%) and CH (23%). H_2 is also formed through

$$CH_3 + O \rightarrow CO + H_2 + H, \quad (15)$$

contributing 16% to H_2 production. The final long-lived species shown in Fig. 3(a) is H_2O_2, formed by the three-body

03 January 2025 12:38:27

© Author(s) 2025

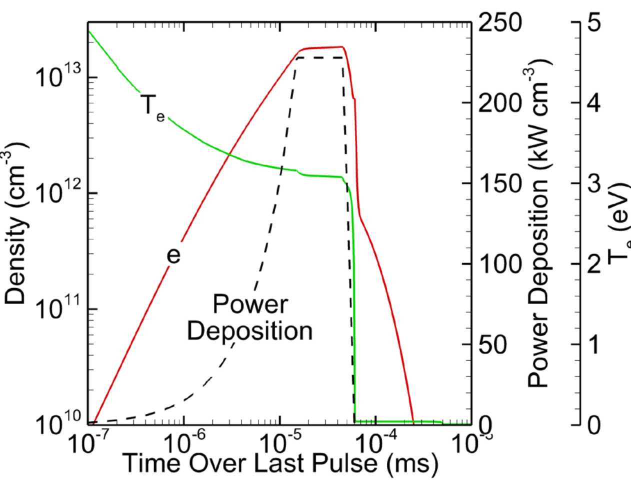

FIG. 1. Electron density and T_e of the $Ar/CH_4/O_2 = 50/25/25$ discharge over the last of 20 pulses. Power deposition is shown for reference.

recombination of OH (55% contribution) as well as

$$HO_2 + HO_2 \rightarrow H_2O_2 + O_2, \tag{16}$$

contributing 41% to H_2O_2 production. While OH forms H_2O_2, OH can also consume H_2O_2 through

$$OH + H_2O_2 \rightarrow H_2O + HO_2, \tag{17}$$

contributing 94% to H_2O_2 consumption.

The long-lived hydrocarbons formed in the plasma are shown in Fig. 3(b). The most abundant long-lived hydrocarbon is C_2H_4 (ethylene). C_2H_4 is produced by CH reacting with CH_4 (65%) and charge-exchange between $C_2H_5^+$ and H_2O (30%). The next most abundant long-lived hydrocarbon is C_2H_6 (ethane), formed dominantly from mutual reactions of CH_3 (98%). While mutual reactions of CH_3 are the dominant production mechanism of C_2H_6, this process only consumes 0.4% of CH_3 in the plasma. Instead of forming C_2H_6 as would be the dominant loss mechanism for CH_3 in an Ar/CH_4 plasma, CH_3 is converted into oxygenated species. C_2H_6 is consumed at an order of magnitude lower rate than the integrated rate by H abstraction with OH to form H_2O. The final C_2H_x species formed in abundance is C_2H_2 (acetylene), produced in multiple electron-ion recombination reactions with $C_2H_5^+$ (42% total). While the C_2H_x species are the most abundant long-lived hydrocarbons, C_3H_x species are also formed. C_3H_8 (propane) is formed by the association of CH_3 and C_2H_5 (99.3%). C_3H_6 (propene) is formed by the association of CH_2 and C_2H_4 (90%) and is consumed in reactions with O by

$$C_3H_6 + O \rightarrow C_2H_5 + CHO, \tag{18}$$

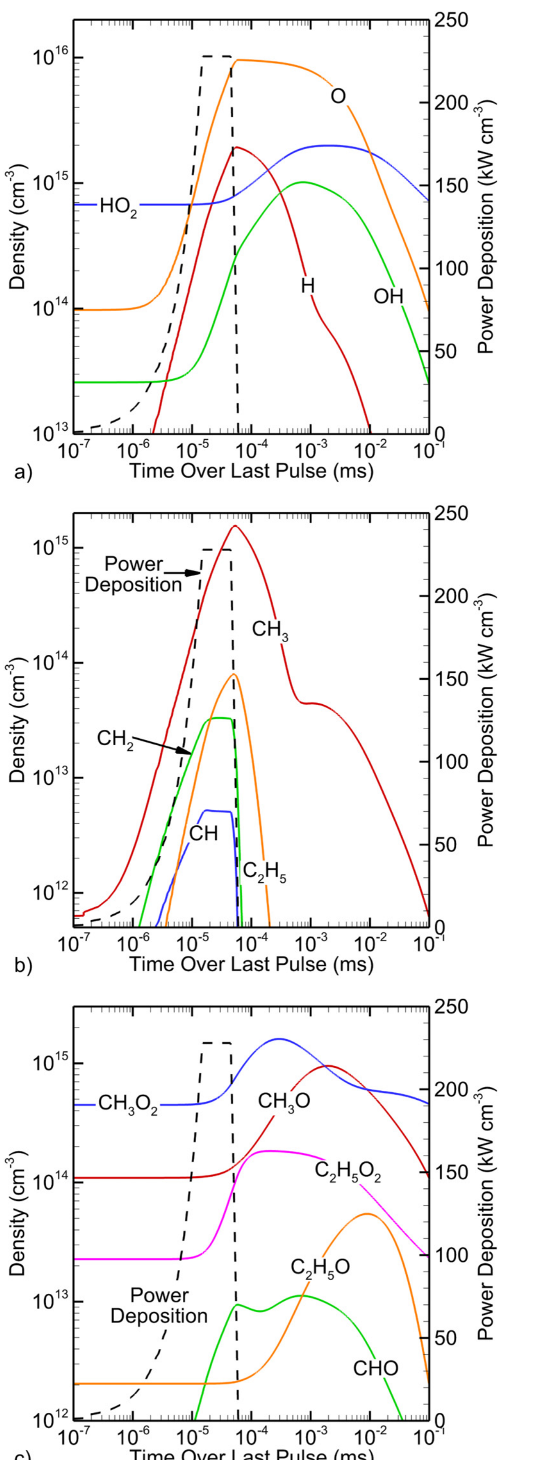

FIG. 2. Radicals generated in the $Ar/CH_4/O_2 = 50/25/25$ discharge over the last of 20 pulses. (a) Reactive oxygen species (ROS) radicals, (b) hydrocarbon radicals, and (c) oxygenated radicals.

03 January 2025 12:38:27

© Author(s) 2025

FIG. 3. Long-lived species generated in the $Ar/CH_4/O_2 = 50/25/25$ discharge over 20 pulses. (a) Non-carbon containing species, (b) hydrocarbon species, and (c) oxygenated species.

$$C_3H_6 + O \rightarrow CH_2CO + CH_3 + H. \tag{19}$$

Reaction (18) contributes 58% to C_3H_6 consumption, while reaction (19) contributes 41%.

The long-lived oxygenated species formed in the plasma are shown in Fig. 3(c). The most abundant long-lived oxygenates are CO, CH_3OH, and CH_2O. CO is the most abundant after 20 pulses with a final density of $3.8 \times 10^{16}\,cm^{-3}$. CO is primarily formed from H abstraction by O_2 from CHO (93%). As O_2 is a feedstock gas, this reaction is limited by the availability of CHO. The CO/H_2 ratio, relevant for syngas applications, reaches 4.3 at the end of 20 pulses. CH_3OH has a density of $2.1 \times 10^{16}\,cm^{-3}$ after 20 pulses. CH_3OH is produced by H abstraction from CH_3O by CH_3O (53%) and O removal from CH_3O_2 (45%). The rates of these reactions are shown over the last pulse in Fig. 4(a). The peak rates occur at different times, attributed to when the densities of the reactants peak. The formation of CH_3O_2 occurs by CH_3 association with O_2, while CH_3O requires CH_3O_2 to form. Therefore, the formation of CH_3OH from CH_3O occurs at a later time than the formation from CH_3O_2. CH_3OH is consumed in reactions with OH, shown in Fig. 4(b), though these reactions occur at 25% of the rate of CH_3OH formation.

CH_2O reaches a density of $1.4 \times 10^{16}\,cm^{-3}$ after 20 pulses. CH_2O is produced through a variety of reactions. CH_2O is produced by H abstraction from CH_3O by CH_3O (32%), H abstraction from CH_3O (15%), and

$$CH_3O + O \rightarrow CH_2O + OH, \tag{20}$$

$$CH_3 + O \rightarrow CH_2O + H. \tag{21}$$

Reaction (20) contributes 13% to CH_2O formation and reaction (21) contributes 11%. As shown in Fig. 4(c), reaction (21) occurs during the discharge pulse, as both O and CH_3 are produced from the electron-impact dissociation of feedstock gases. The other three reactions that produce CH_2O rely on CH_3O, which reaches its maximum density $2\,\mu s$ after the last pulse begins. As a result, the maximum rates of those reactions occur near $2\,\mu s$. While CH_2O is formed at an integrated rate of $5.6 \times 10^{16}\,cm^{-3}$ over the 20 pulses, $4.0 \times 10^{16}\,cm^{-3}$ of CH_2O is consumed over these 20 pulses. The main consumption mechanisms of CH_2O are CHO formation through H abstraction by OH (79%) and by O (18%), shown in Fig. 4(d). H abstraction by O reaches its maximum rate as the power begins to decrease, corresponding to the maximum in O density. OH, however, is formed later from the reactions of HO_2, and therefore, the rate peaks later at $0.7\,\mu s$.

While CO, CH_3OH, and CH_2O are the most abundant oxygenated species, significant densities of other oxygenated species are also formed. CO_2 is formed from

$$CH_3CO + O \rightarrow CO_2 + CH_3, \tag{22}$$

$$OH + CO \rightarrow CO_2 + H. \tag{23}$$

Reaction (22) contributes 33% of CO_2 formation and reaction (23) contributes 24%. CO_2 reaches a density of $2.3 \times 10^{15}\,cm^{-3}$

03 January 2025 12:38:27

© Author(s) 2025

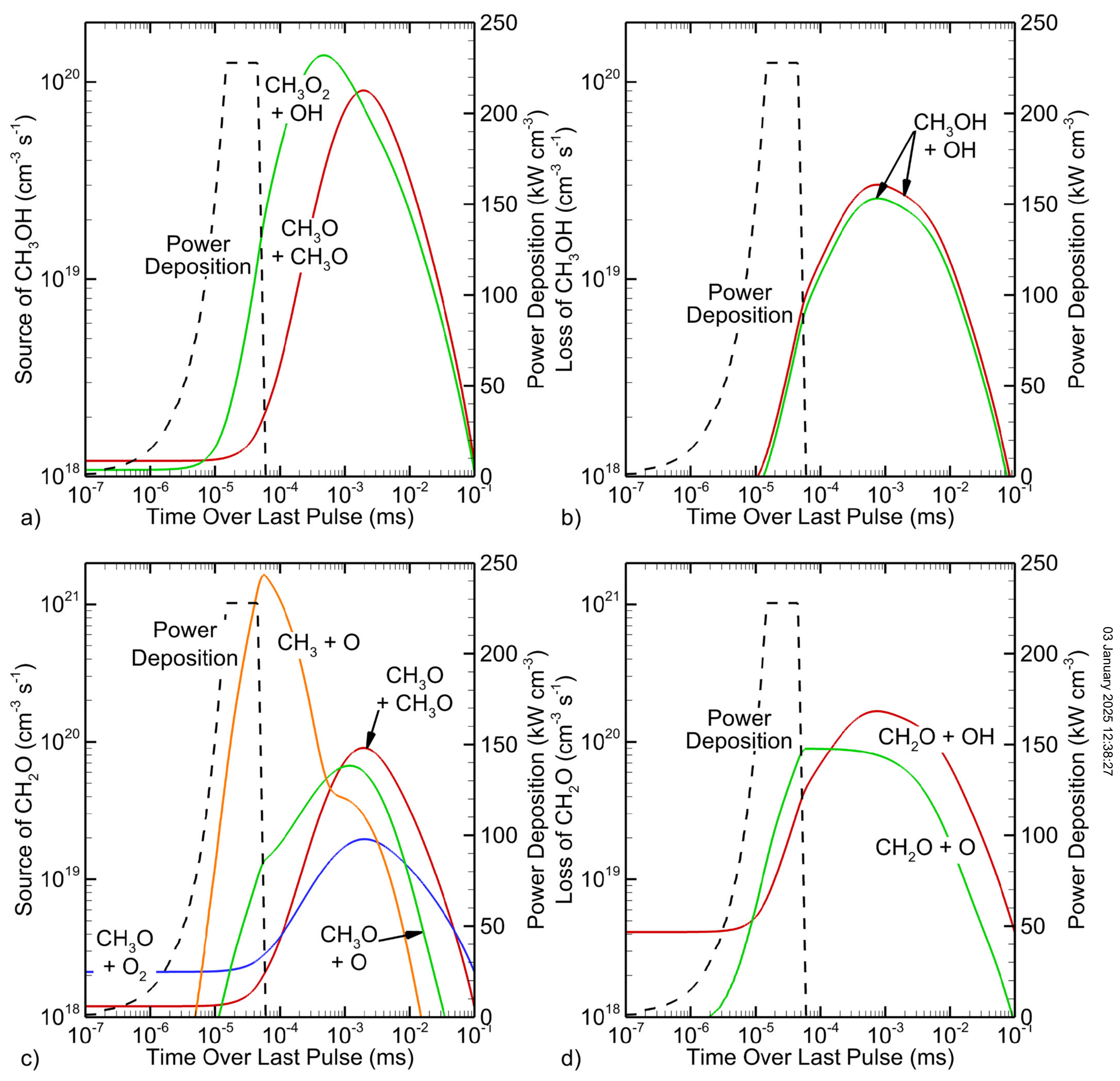

FIG. 4. Rates of CH_3OH and CH_2O production and consumption in the $Ar/CH_4/O_2$ = 50/25/25 discharge over the last of 20 pulses. (a) CH_3OH production, (b) CH_3OH consumption, (c) CH_2O production, and (d) CH_2O consumption. Note that the consumption and production rates for each species are shown on the same scale.

03 January 2025 12:38:27

after 20 pulses, an order of magnitude less than CO. However, as CO_2 is a greenhouse gas, its production is not desirable. CH_3OOH (methyl hydroperoxide) is formed by CH_3O_2 reacting with HO_2 (94%). C_2H_5OH (ethanol) is also formed in the plasma. Similar to CH_3OH, C_2H_5OH is formed by the reactions between OH and $C_2H_5O_2$ (96%). CH_3CHO (acetaldehyde) is produced by

$$C_2H_5O + O_2 \rightarrow CH_3CHO + HO_2, \tag{24}$$

© Author(s) 2025

contributing 95% of CH_3CHO production. CH_3CHO is produced with an integrated rate of $2.3 \times 10^{15}\,cm^{-3}$ while its consumption totals to $1.7 \times 10^{15}\,cm^{-3}$. The dominant consumption mechanisms of CH_3CHO are H abstraction by OH (69%) and O (26%). The final oxygenated species shown in Fig. 3(c) is C_2H_5OOH (ethyl hydroperoxide), produced by

$$C_2H_5O_2 + HO_2 \rightarrow C_2H_5OOH + O_2, \tag{25}$$

contributing 91% to C_2H_5OOH production. C_2H_5OOH is produced with an integrated rate of $3.8 \times 10^{14}\,cm^{-3}$ and consumed at $1.2 \times 10^{14}\,cm^{-3}$ through H abstraction by OH (58%) and O (41%).

IV. GAS MIXTURES

A goal of this study is to determine the conditions that maximize the density of CH_3OH (and, to a lesser extent, CH_2O) while minimizing the amount of CO_2 formed. The gas mixture in which the plasma is sustained affects the fundamental plasma properties (electron density, T_e), as well as the long-lived species formed and their relative concentrations. In Sec. IV A, the fraction of Ar in the mixture is varied while holding the ratio CH_4/O_2 constant at 1/1. In Sec. IV B, the ratio of CH_4/O_2 is changed while keeping a constant 50% Ar mole fraction.

A. Ar dilution

Previous studies have shown that increasing the noble gas content in CH_4/CO_2 plasmas increases the conversion of CH_4 and CO_2.[18,19,21] In this section, the effect of changing the Ar percentage while keeping the CH_4/O_2 ratio constant at 1/1 as in the base case is examined.

As the Ar percentage increases from 0% to 95% Ar, the electron density when the power begins to decrease over the last pulse (45 ns) increases from 9.4×10^{12} to $7.9 \times 10^{13}\,cm^{-3}$. With the increase in Ar, T_e increases from 2.98 to 3.27 eV. During the quasi-steady state, electron temperature is determined by the balance of ionization sources and charged particle losses. With the power profile being held constant, electron density is then determined by the power dissipation per electron at the self-sustaining electron temperature. The first inelastic electron-impact threshold with Ar is electronic excitation at an energy of 11.55 eV, while the ionization threshold is 16 eV. With Ar dilution, the mole-fraction weighted power dissipation per electron decreases as the rate of power dissipation by electrons with CH_4 or O_2 is larger due to their rotational–vibrational modes and lower threshold energies for electronic excitation and ionization. This condition is somewhat mediated at high power deposition when multistep ionization of argon begins to dominate, and at intermediate mole fractions of the molecular gas when Penning processes can be important.

The frequency of radical formation by electron-impact on a molecular species is $f_r = n_e \sum_i k_i(T_e)$, where the sum is over rate coefficients for radical formation. The total rate of radical formation by, for example, electron-impact on CH_4 is $f_t = n_e[CH_4] \sum_i k_i(T_e)$. With the increases in electron temperature and density with Ar dilution, f_r monotonically increases while

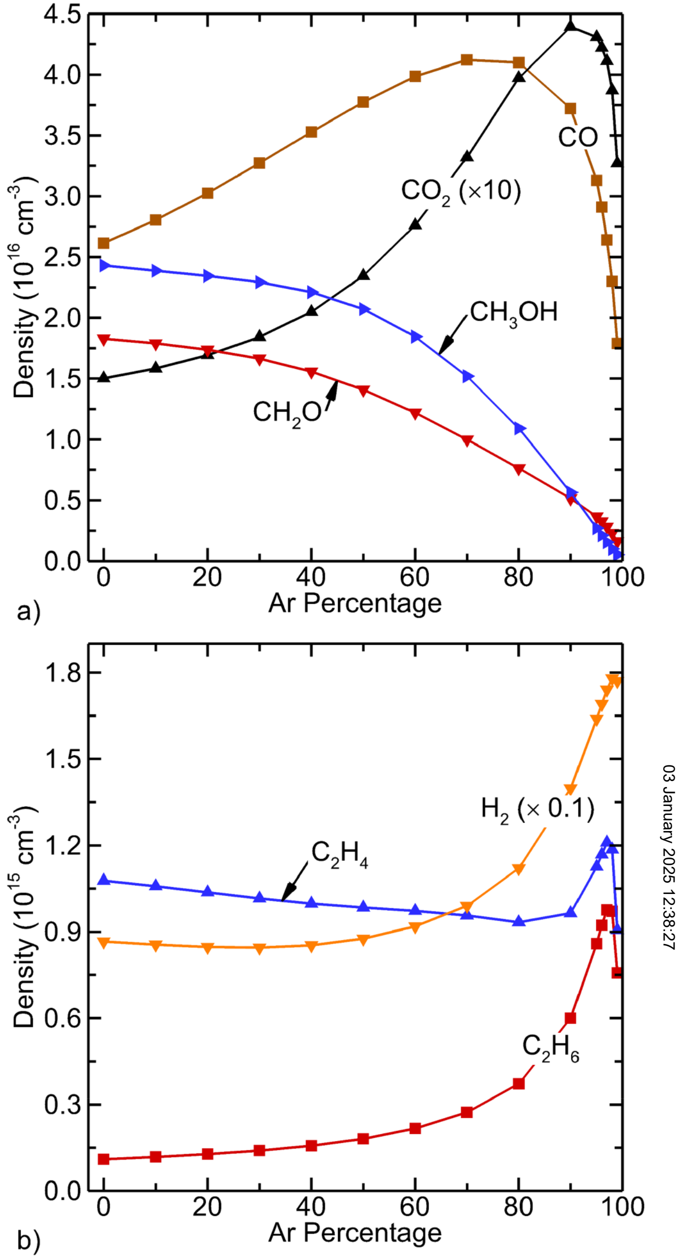

FIG. 5. Consequences of changing the Ar percentage in the gas mixture while keeping $CH_4/O_2 = 1/1$. (a) Long-lived oxygenates densities and (b) long-lived hydrocarbon species densities. Values are the maximum densities over the last of 20 pulses.

03 January 2025 12:38:27

$[CH_4]$ monotonically decreases. These trends result in f_t being maximum at an intermediate Ar dilution.

The maximum oxygenated species densities (CH_3OH, CH_2O, CO, and CO_2) over the last pulse are shown in Fig. 5(a) as a

© Author(s) 2025

function of Ar percentage. CH_3OH and CH_2O both decrease as the Ar percentage increases. For CH_3OH, the decrease is slow below 40%, while above 40% Ar, the decrease becomes more rapid. While the production of CH_3OH due to CH_3O reacting with CH_3O and CH_3O_2 reacting with OH increases up to a 40% Ar mole fraction, the consumption of CH_3OH by OH also increases. The increase in the consumption of CH_3OH outweighs the increase in CH_3OH production, thereby decreasing its density.

Above a mole fraction of 40% Ar, the consumption of CH_3OH by OH continues to increase while the production of CH_3OH decreases, leading to a more rapid decrease in the CH_3OH density. Similarly, CH_2O production relies on CH_3O and CH_3, and increases through 40% Ar. However, the consumption of CH_2O due to OH also increases, thereby outweighing the increase in production to decrease the CH_2O density. Above 40% Ar, the density of CH_2O is not well correlated to the density of CH_3OH. While the production of CH_2O due to CH_3O reactions decreases above 40% Ar, its production due to CH_3 reacting with O increases. Therefore, the decrease in CH_2O production is less pronounced than in CH_3OH.

The production of both CH_3OH and CH_2O relies on the CH_3O radical. The production of CH_3O by CH_3O_2 reacting with O increases up to 40% Ar. CH_3O_2 production by association of CH_3 and O_2 also increases up to 40% Ar, following the production of CH_3 by H abstraction from CH_4. CH_3O_2 and CH_3 production by H abstraction both increase with increasing T_{gas}, with T_{gas} reaching a maximum of 414 K in the afterglow at 40% and 50% Ar.

While the densities of CH_3OH and CH_2O decrease with increasing Ar, the densities of CO and CO_2 increase up to Ar mole fractions of 70%–90%, as shown in Fig. 5(a). CO reaches a maximum density of $4.1 \times 10^{16}\,cm^{-3}$ at 70% Ar, while CO_2 reaches $4.4 \times 10^{15}\,cm^{-3}$ at 90% Ar. CO relies on its production by H abstraction from CHO by O_2, which increases to 70% Ar. CHO is formed by H abstraction from CH_2O by OH. Since CH_2O decreases as Ar increases, the increase in CHO production occurs because of the increase in T_{gas} as well as the increase in OH density. The density of OH increases up to 90% Ar as the production from HO_2 reacting with O increases. This trend prevails in spite of a decrease in OH production from HO_2 reacting with $O_2(^1\Delta)$. CO_2 production from CH_3CO reacting with O and OH reacting with CO increase to 80% Ar and 90% Ar, respectively. These reactions lead to a maximum CO_2 density at 90% Ar.

The long-lived hydrocarbon densities (C_2H_4, C_2H_6, and H_2) are shown in Fig. 5(b). The trends are different than the oxygenated species. The maximum in all the long-lived hydrocarbon densities occurs at 97%–98% Ar. These counter-intuitive trends result largely from the increase in electron density and rate coefficients for electron-impact processes, leading to the formation of long-lived hydrocarbons increasing more rapidly than the decrease in CH_4 density. H_2 remains relatively constant from 0% to 50% Ar and increases after 50% Ar. However, H_2 production from the electron-impact dissociation of CH_4 decreases as the mole fraction of Ar increases as there is less CH_4 in the discharge. Therefore, for the H_2 density to increase, the source of H_2 from other reactions must increase. H_2 production from other reactions, including CH_3 reacting with O, increases with the increasing Ar percentage. Other reactions contributing to H_2 production that were not identified at 50% Ar become important after 70% Ar. These reactions include

$$H + HO_2 \rightarrow H_2 + O_2, \tag{26}$$

$$CH_3O + H \rightarrow CH_2O + H_2. \tag{27}$$

The density of C_2H_4 exhibits a small decrease from 0% Ar to 80% Ar before increasing to 97% Ar. The production of C_2H_4 from CH reacting with CH_4 decreases with the increasing Ar percentage, but the production from $C_2H_5^+$ reacting with H_2O and from H abstraction from C_2H_5 increases. That increase offsets the decrease from CH reacting with CH_4. For mole fractions larger than 80% Ar, the production from $C_2H_5^+$ reacting with H_2O and H abstraction from C_2H_5 further increases, driving an increase in C_2H_4 density. The density of C_2H_6 increases with increasing Ar mole fraction to 97%, though the increase becomes more rapid after 50% Ar. C_2H_6 is produced dominantly by the mutual association of CH_3, and the maximum CH_3 density over the last pulse increases nearly linearly with the Ar percentage from $1.4 \times 10^{15}\,cm^{-3}$ at 0% Ar to $1.8 \times 10^{13}\,cm^{-3}$ at 95% Ar. After 97%–98% Ar, H_2, C_2H_4, and C_2H_6 densities decrease as CH_4 makes up less than 3% of the discharge—the increase in plasma density and electron temperature with increasing Ar mole fraction cannot compensate for the low mole fraction of CH_4.

The fraction of the inlet O_2 remaining is between 70% and 80% for the change in Ar content shown in Fig. 5. On that basis alone, one might expect that the production of, for example, CH_3OH and CH_2O would decrease based on there being fewer O atoms available due to the depletion of the O_2 feedstock. However, the degree of dissociation of O_2 does not straightforwardly increase or decrease the production of CH_3OH and CH_2O. There should clearly be sufficient O atom production to enable the stoichiometry of the products. However, one of the eventual products of O_2 dissociation is OH which is involved in both the production and consumption reactions of CH_2O and CH_3OH. At some intermediate degree of O_2 dissociation, sufficient O atoms are produced while not also feeding the destruction pathways.

These results indicate that for the ratio of $CH_4/O_2 = 1/1$, operating with a small Ar mole fraction will maximize the CH_3OH and CH_2O densities while producing little CO_2. In fact, at 95% Ar, the density of CO_2 is larger than the density of either CH_3OH or CH_2O. These trends are, however, sensitive to the ratio of CH_4/O_2.

B. Ratio of CH_4 and O_2

Ultimately, the production of oxygenates depends on the reactions between carbon-containing and oxygen-containing species, while higher order hydrocarbon production depends largely on the reactions between non-oxygen containing species. In this regard, the branching to different oxygenated and hydrocarbon products likely depends on the ratio of CH_4 to O_2 in the mixture. In this section, these trends are discussed while the Ar mole fraction is held constant at 50%, and the CH_4 and O_2 percentages are varied. At low CH_4 percentages (high O_2 percentages), oxygenate formation is expected to dominate over hydrocarbon formation as oxygen is abundant. At high CH_4 percentages (low O_2

03 January 2025 12:38:27

© Author(s) 2025

percentages), hydrocarbon formation is expected to dominate over oxygenate formation as oxygen is less abundant.

The electron density as the last power pulse begins to ramp down (45 ns) increases from $1.3 \times 10^{13}\,cm^{-3}$ at 5% CH_4 to $3.4 \times 10^{13}\,cm^{-3}$ at 45% CH_4. This increase is due, in part, to decreased negative ion formation, with the maximum total negative ion density occurring at 20% CH_4. The negative ions are dominantly the negative water cluster ions $O_2^-(H_2O)$, $O_2^-(H_2O)_2$, and $O^-(H_2O)$ that follow the formation of O_2^- and O^-. While the maximum densities of O_2^- and O^- occur at 5% CH_4 (45% O_2), the maximum of the cluster ion densities occurs at 20% CH_4 as H_2O is formed in the discharge instead of being present as one of the feedstock gases. While the electron density increases, T_e decreases from 3.21 eV at 5% CH_4 to 2.85 eV at 45% CH_4.

The dominant long-lived species are shown in Fig. 6 with the oxygenates shown in Fig. 6(a) as a function of CH_4 and O_2 percentage. CH_3OH and CH_2O reach their maximum densities at 35% and 40% CH_4, respectively. This is surprising because the O_2 content in the discharge is low (10%–15%). The production of both CH_3OH and CH_2O by CH_3O reacting with CH_3O increases to 35% CH_4 which explains the maximum CH_3OH density at 35% CH_4. However, CH_2O reaches a maximum at 40% CH_4 due to its additional production from CH_3 reacting with O increasing to 40% CH_4. Both CH_3OH and CH_2O production rely on CH_3O. The maximum CH_3O density occurs at 30% CH_4, based largely on the production from CH_3O_2 which reaches a maximum at 25% CH_4. The CH_3O_2 density is maximum at 30%–35% CH_4. While the density of CH_3 reaches a maximum at 40% CH_4, the association reaction to form CH_3O_2 depends on T_{gas}, which reaches its maximum at 25% CH_4 (414 K).

The fraction of inlet O_2 remaining is between 70% and 80% for the changing CH_4/O_2 content shown in Fig. 6 while the production of CH_3OH and CH_2O is maximum for an O_2 inlet flow of 10–15%. The small amount of O_2 at this maximum in production may be counterintuitive. The production of CH_3OH and CH_2O generally requires CH_3O as a precursor. CH_3O is produced from CH_3O_2, which is generated by the reactions between $CH_3 + O_2$. The CH_3 content is critical for CH_3OH and CH_2O production and can be the rate-limiting step, provided, there is a critical amount of O_2 remaining.

The densities of CO and CO_2 follow a different trend than those of CH_3OH and CH_2O. These species are formed preferentially at low CH_4 percentages, with densities reaching a maximum at 20% CH_4 (30% O_2). The maximum in CO density follows the maximum of its production from H abstraction from CHO by O_2. CHO is produced by H abstraction from CH_2O by either OH or O. The rates of these reactions increase to 20%–25% CH_4 due to the increase in both CH_2O density and T_{gas}. The production mechanisms of CO_2 (OH reacting with CO and CH_3CO reacting with O) reach their maximum at less than 25% CH_4, leading to a maximum CO_2 density at 20% CH_4.

The densities of long-lived hydrocarbons and H_2 are shown in Fig. 6(b). As expected, these species increase with increasing CH_4, as they do not require oxygen to form. In fact, their production is enhanced since the hydrocarbon radicals which would otherwise be consumed by forming oxygenates are more readily available for hydrocarbon formation as the fraction of O_2 decreases. H_2 and C_2H_4 both reach their maximum density at 40% CH_4. H_2 is produced primarily from the electron-impact dissociation of CH_4. While T_e decreases as the CH_4 percentage increases, the electron and CH_4 densities increase. These increases lead to an increase in the rate of electron-impact dissociation of CH_4 through 40% CH_4.

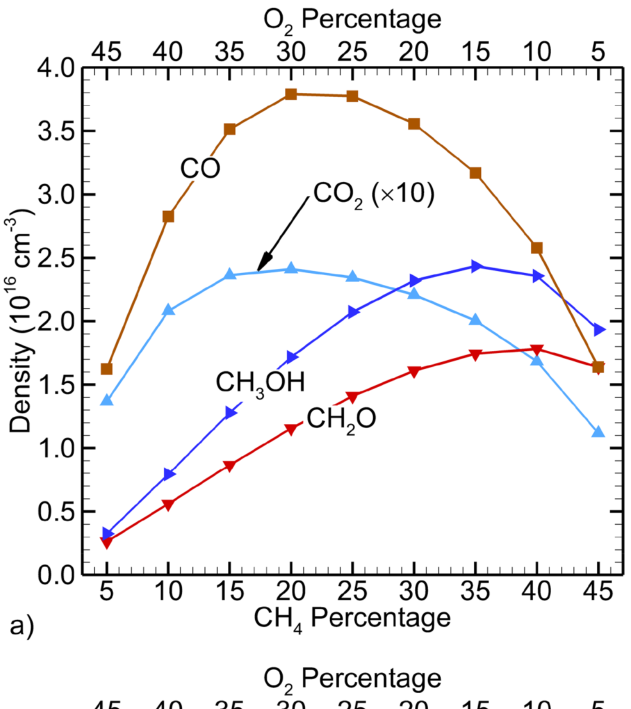

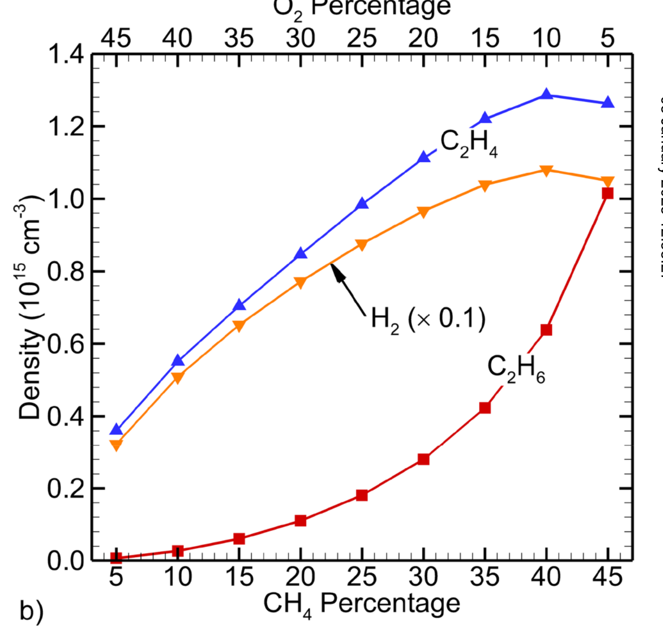

FIG. 6. Consequences of CH_4 and O_2 percentages while keeping a 50% Ar mole fraction. (a) Long-lived oxygenates densities and (b) long-lived hydrocarbon species densities. Values are the maximum over the last 20 pulses.

03 January 2025 12:38:27

© Author(s) 2025

The production of C_2H_4 by $C_2H_5^+$ reacting with H_2O decreases above 15% CH_4, but the production by CH reacting with CH_4 increases. This increase occurs as the rate of electron-impact dissociation of CH_4 producing CH increases to 40% CH_4. The density of C_2H_6 increases through 45% CH_4 which is primarily formed through mutual reactions of CH_3. The integrated rate of mutual association of CH_3 increases from $8.4 \times 10^{12}\,cm^{-3}$ at 5% CH_4 to $1.1 \times 10^{15}\,cm^{-3}$ at 45% CH_4.

Increasing the CH_4/O_2 ratio with a constant mole fraction of 50% Ar increases the production of CH_3OH and CH_2O and simultaneously decreases CO_2. The results presented in this section show that at 50% Ar, 35%–40% CH_4 (10%–15% O_2) optimize CH_3OH and CH_2O production. At these conditions, the production of CO_2 decreases relative to its concentration at $CH_4/O_2 = 1/1$.

Although not a direct focus of this investigation, plasma conditions can be optimized to generate specific end products. For example, CH_3CHO (acetaldehyde) is widely used as an intermediate to generate acetic acid, peracetic acid, pyridine bases, and other chemicals. The production of CH_3CHO from ethylene[35] by the Wacker process is one of the most important processes in the chemical industry,[36] while acetaldehyde is itself a hazardous liquid. Less capital intensive and safer, point-of-use production of CH_3CHO would be advantageous for on-demand organic syntheses. For our setup, plasma generation of CH_3CHO is maximum for conditions similar to those of the other C_2 compounds. For 50% argon mixtures, CH_3CHO production is maximum with 40% CH_4 (10% O_2) resulting in a density of $8 \times 10^{14}\,cm^{-3}$ after 20 pulses. For a ratio of $CH_4/O_2 = 1/1$, CH_3CHO production is maximum in the absence of argon, generating a density of $6 \times 10^{14}\,cm^{-3}$ after 20 pulses.

V. CONVERSION AND ENERGY EXPENDITURE

The intent of this investigation was to address reaction mechanisms and not necessarily optimize conversion and energy efficiency for CH_4 oxygenation. Although global modeling is well suited to discussions of mechanisms, often, energy efficiencies are dependent on geometrical considerations that are difficult to include in global models—such as division in power deposition between sheaths and bulk, propagation of streamers or surface ionization waves, and gas flow (replenishment and pumping of gases).

That said, some assessments can be made. The conversion rates of CH_4 and O_2 were assessed for a sealed-off system to eliminate the uncertainties in accounting for gas flow and pressure stabilization while varying the CH_4/O_2 ratio with 50% Ar. The maximum CH_4 conversion was 2.2% at 5% CH_4, decreasing to 0.7% for 45% CH_4. The maximum O_2 conversion was 6.4% at 5% O_2, decreasing to 3.0% for 45% O_2. Xu and Tu measured CH_4 conversion in an AC DBD with pure CH_4 and reported a conversion percentage of 25.2% at the longest residence time (16 s).[37] Chen *et al.* reported a maximum conversion of 31.9% in a pure CH_4 nanosecond pulsed DBD.[38] Jo *et al.* reported a CH_4 conversion percentage of 7%–11% for $Ar/CH_4/O_2$ plasmas in an AC DBD for varying O_2 and CH_4 concentrations.[22] As these rates of conversion are dependent on residence time and energy deposition-per-molecule, direct comparisons are better made normalized by energy deposition.

The energy required for conversion (expressed as eV/molecule) was evaluated in a sealed-off system while varying the CH_4/O_2 ratios at 50% Ar. For these conditions, the minimum energy cost for the conversion of CH_4 was 13.8 eV/molecule for $Ar/CH_4/O_2 = 50/30/20$. Xu and Tu measured a maximum energy efficiency of 0.26 mmol/kJ (40 eV/molecule) for CH_4 conversion in an AC DBD operating in pure CH_4.[37] While the calculated energy cost in this work was lower than that reported in Xu and Tu, the plasma in this work was formed in $Ar/CH_4/O_2$ instead of pure CH_4. The calculated energy cost for the production of CH_3OH was minimum at $Ar/CH_4/O_2 = 50/35/15$ at 46.6 eV/molecule. Wang *et al.* reported a maximum energy efficiency of CH_3OH production of 0.83 mol/kWh (45 eV/molecule) in an AC DBD operating in CH_4/CO_2,[23] comparable to the calculated energy cost in this work.

VI. CONCLUDING REMARKS

The formation of value-added chemicals in atmospheric pressure plasmas can provide an alternative to energy-intensive steam and dry reforming of CH_4. The production of oxygenates, including CH_3OH and CH_2O, using plasmas sustained in $Ar/CH_4/O_2$ was investigated using a 0D plasma chemistry model *GlobalKin*. The geometry was focused on narrow channels as might be used in microfluidic devices where a scale is achieved by massively parallel sets of microchannels. The goal of this study was to investigate reaction mechanisms resulting in the production of CH_3OH and CH_2O while minimizing the production of the greenhouse gas CO_2.

First, the plasma chemistry in $Ar/CH_4/O_2 = 50/25/25$ was examined. Of the many radical species that are formed in the plasma, CH_3 and O are formed directly by the electron-impact dissociation of CH_4 and O_2. Others, particularly the oxygenated radicals CH_3O_2, CH_3O, and CHO, depend on those initial radicals for their formation. Further reaction of these species branch to several products. The oxygenates, including CO, CH_3OH, and CH_2O, comprise most of the carbon-containing products while the greenhouse gas CO_2 is also formed. Pure hydrocarbon products (C_2H_4 and C_2H_6) are also formed, albeit at an order of magnitude of lower density. The formation of CH_3OH relies on CH_3O and CH_3O_2, while the formation of CH_2O relies on CH_3O and CH_3. CO is formed almost exclusively by H abstraction from CHO.

The mole fractions of the feed gas affect the selectivity of the process and, in particular, the production of CH_3OH, CH_2O, and CO_2. First, the consequences of Ar percentage were examined while keeping the ratio $CH_4/O_2 = 1/1$. CH_3OH and CH_2O have maximum densities at 0% Ar, while the density of CO is the highest at 70% Ar and CO_2 is the highest at 90% Ar. If the goal is, for example, CO production for syngas, moderate Ar additions are beneficial. However, if the goal is CH_3OH or CH_2O, Ar dilution is not beneficial. When varying the CH_4/O_2 ratio at a constant 50% Ar, the densities of CH_3OH and CH_2O are maximum at 35%–40% CH_4 (10%–15% O_2) while the densities of CO and CO_2 are the maximum at 20% CH_4. Therefore, a CH_4 rich discharge of 35%–40% favors CH_3OH and CH_2O production while minimizing CO_2 formation.

Conventional microfluidic labs-on-a-chip are intentionally designed to have long residence times (many to tens of seconds or more), a goal achieved with channel lengths of up to several meters. Although optimum for microfluidic processing, this is not necessarily the geometry that would be implemented for plasma conversion using microchannels. With these long channel lengths

03 January 2025 12:38:27

© Author(s) 2025

and residence times, the desired products would also be subject to lengthy electron-impact dissociation and ionization. An advantage of plasma conversion using microchannels is that the precise time of plasma exposure can be set by the length of the channel and gas flow. Although not the focus of this investigation, we anticipate that optimized plasma conversion using microchannels would consist of large arrays of parallel channels, with residence time in any given channel being tens to hundreds of ms. These parameters would be chosen to optimize the conversion of the feedstock gas while not detrimentally undergoing plasma dissociation of the desired products.

SUPPLEMENTARY MATERIAL

See the supplementary material for additions and revisions to the prior published reaction mechanism[33] for plasmas sustained in Ar/CH_4 mixtures to account for the addition of oxygen.

ACKNOWLEDGMENTS

This material was based upon work supported by the National Science Foundation under Award Nos. ECO-CBET-2032604 and ECO-CBET-2032664. Any opinions, findings, and conclusions or recommendations expressed in this material are those of the author(s) and do not necessarily reflect the views of the National Science Foundation. This work was also supported by the Department of Energy Office of Fusion Energy Sciences (No. DE-SC0020232) and the Army Research Office MURI program (No. W911NF-20-1-0105).

AUTHOR DECLARATIONS

Conflict of Interest

The authors have no conflicts of interest.

Author Contributions

Mackenzie Meyer: Conceptualization (lead); Data curation (lead); Formal analysis (lead); Investigation (lead); Methodology (equal); Writing – original draft (lead); Writing – review & editing (equal). **Ryan Hartman:** Funding acquisition (equal); Project administration (equal); Supervision (equal); Writing – review & editing (equal). **Mark J. Kushner:** Formal analysis (supporting); Funding acquisition (equal); Investigation (supporting); Methodology (equal); Project administration (equal); Resources (equal); Supervision (equal); Writing – review & editing (equal).

DATA AVAILABILITY

The data that support the findings of this study are available from the corresponding author upon reasonable request.

REFERENCES

[1]J. H. Lunsford, Catal. Today **63**, 165 (2000).
[2]T. Mokrani and M. Scurrell, Catal. Rev. **51**, 1–145 (2009).
[3]E. Morais and A. Bogaerts, Plasma Process. Polym **21**, 2300149 (2023).
[4]P.-A. Maitre, M. S. Bieniek, and P. N. Kechagiopoulos, Chem. Eng. Sci. **234**, 116399 (2021).
[5]W. Wang, R. Snoeckx, X. Zhang, M. S. Cha, and A. Bogaerts, J. Phys. Chem. C **122**, 8704 (2018).
[6]T. Miura, K. Takahashi, K. Takaki, and Y. Nishida, IEEE Trans. Plasma Sci. **49**, 147 (2021).
[7]S. Heijkers, M. Aghaei, and A. Bogaerts, J. Phys. Chem. C **124**, 7016 (2020).
[8]C. Montesano, M. Faedda, L. M. Martini, G. Dilecce, and P. Tosi, J. CO_2 Util. **49**, 101556 (2021).
[9]D. Mei, P. Zhang, G. Duan, S. Liu, Y. Zhou, Z. Fang, and X. Tu, J. CO_2 Util. **62**, 102073 (2022).
[10]C. Bai, L. Wang, L. Li, X. Dong, Q. Xiao, Z. Liu, J. Sun, and J. Pan, AIP Adv. **9**, 035023 (2019).
[11]R. Snoeckx, R. Aerts, X. Tu, and A. Bogaerts, J. Phys. Chem. C **117**, 4957 (2013).
[12]A. Ozkan, T. Dufour, G. Arnoult, P. D. Keyzer, A. Bogaerts, and F. Reniers, J. CO_2 Util. **9**, 74 (2015).
[13]E. Cleiren, S. Heijkers, M. Ramakers, and A. Bogaerts, ChemSusChem **10**, 4025 (2017).
[14]B. Wanten, S. Maerivoet, C. Vantomme, J. Slaets, G. Trenchev, and A. Bogaerts, J. CO_2 Util. **56**, 101869 (2022).
[15]L. Zhang, S. Heijkers, W. Wang, L. M. Martini, P. Tosi, D. Yang, Z. Fang, and A. Bogaerts, Plasma Sources Sci. Technol. **31**, 055014 (2022).
[16]M. Ramakers, I. Michielsen, R. Aerts, V. Meynen, and A. Bogaerts, Plasma Process. Polym. **12**, 755 (2015).
[17]T. Y. Chen, A. C. Rousso, S. Wu, B. M. Goldberg, H. van der Meiden, Y. Ju, and E. Kolemen, J. Phys. D: Appl. Phys. **52**, 18LT02 (2019).
[18]N. R. Pinhão, A. Janeco, and J. B. Branco, Plasma Chem. Plasma Process. **31**, 427 (2011).
[19]V. Goujard, J.-M. Tatibouët, and C. Batiot-Dupeyrat, Plasma Chem. Plasma Process. **31**, 315 (2011).
[20]A. Janeco, N. R. Pinhão, and V. Guerra, J. Phys. Chem. C **119**, 109 (2015).
[21]A. Rahmani and M. Nikravech, Plasma Chem. Plasma Process. **38**, 517 (2018).
[22]S. Jo, D. Hoon Lee, and Y.-H. Song, Chem. Eng. Sci. **130**, 101 (2015).
[23]Y. Wang, Y. Chen, J. Harding, H. He, A. Bogaerts, and X. Tu, Chem. Eng. J. **450**, 137860 (2022).
[24]C. De Bie, J. van Dijk, and A. Bogaerts, J. Phys. Chem. C **119**, 22331 (2015).
[25]A. N. Biswas, L. R. Winter, B. Loenders, Z. Xie, A. Bogaerts, and J. G. Chen, ACS Energy Lett. **7**, 236 (2022).
[26]T. Kolb, J. H. Voigt, and K.-H. Gericke, Plasma Chem. Plasma Process. **33**, 631 (2013).
[27]S. Li, J. Sun, Y. Gorbanev, K. van't Veer, B. Loenders, Y. Yi, T. Kenis, Q. Chen, and A. Bogaerts, ACS Sustain. Chem. Eng. **11**, 15373 (2023).
[28]B. Loenders, Y. Engelmann, and A. Bogaerts, J. Phys. Chem. C **125**, 2966 (2021).
[29]Y. Wang, L. Fan, H. Xu, X. Du, H. Xiao, J. Qian, Y. Zhu, X. Tu, and L. Wang, Appl. Catal., B **315**, 121583 (2022).
[30]S. Liu, L. R. Winter, and J. G. Chen, ACS Catal. **10**, 2855 (2020).
[31]A. M. Lietz and M. J. Kushner, J. Phys. D: Appl. Phys. **49**, 425204 (2016).
[32]W. Van Gaens and A. Bogaerts, J. Phys. D: Appl. Phys. **46**, 275201 (2013).
[33]M. Meyer, S. Kerketta, R. Hartman, and M. J. Kushner, J. Phys. Chem. A **128**, 2656 (2024).
[34]D. L. Baulch, C. T. Bowman, C. J. Cobos, R. A. Cox, T. Just, J. A. Kerr, M. J. Pilling, D. Stocker, J. Troe, W. Tsang, R. W. Walker, and J. Warnatz, J. Phys. Chem. Ref. Data **34**, 757 (2005).
[35]Y. Chen, M. J. Kuo, R. Lobo, and M. Ierapetritou, Green Chem. **26**, 2903 (2024).
[36]R. Jira, Angew. Chem., Int. Ed. **48**, 9034 (2009).
[37]C. Xu and X. Tu, J. Energy Chem. **22**, 420 (2013).
[38]X. Chen, S. Zhang, S. Li, C. Zhang, J. Pan, A. B. Murphy, and T. Shao, Sustain. Energy Fuels **5**, 787 (2021).

03 January 2025 12:38:27

© Author(s) 2025